Methods in ENZYMOLOGY

Volume 703

Mononuclear non-heme iron dependent enzymes Part A

Edited by

Jennifer Bridwell-Rabb

VOLUME SEVEN HUNDRED AND THREE

METHODS IN **ENZYMOLOGY**

Mononuclear Non-heme Iron Dependent Enzymes Part A

METHODS IN ENZYMOLOGY

Editors-in-Chief

ANNA MARIE PYLE

Departments of Molecular, Cellular and Developmental Biology and Department of Chemistry
Investigator, Howard Hughes Medical Institute
Yale University

DAVID W. CHRISTIANSON

Roy and Diana Vagelos Laboratories
Department of Chemistry
University of Pennsylvania
Philadelphia, PA

Founding Editors

SIDNEY P. COLOWICK and NATHAN O. KAPLAN

VOLUME SEVEN HUNDRED AND THREE

METHODS IN ENZYMOLOGY

Mononuclear Non-heme Iron Dependent Enzymes Part A

Edited by

JENNIFER BRIDWELL-RABB
Department of Chemistry, University of Michigan, Ann Arbor, MI, United States

ACADEMIC PRESS
An imprint of Elsevier

Academic Press is an imprint of Elsevier
50 Hampshire Street, 5th Floor, Cambridge, MA 02139, United States
525 B Street, Suite 1650, San Diego, CA 92101, United States
125 London Wall, London, EC2Y 5AS, United Kingdom

First edition 2024

Notices

Knowledge and best practice in this field are constantly changing. As new research and experience broaden our understanding, changes in research methods, professional practices, or medical treatment may become necessary.

Practitioners and researchers must always rely on their own experience and knowledge in evaluating and using any information, methods, compounds, or experiments described herein. In using such information or methods they should be mindful of their own safety and the safety of others, including parties for whom they have a professional responsibility.

To the fullest extent of the law, neither the Publisher nor the authors, contributors, or editors, assume any liability for any injury and/or damage to persons or property as a matter of products liability, negligence or otherwise, or from any use or operation of any methods, products, instructions, or ideas contained in the material herein.

ISBN: 978-0-443-31304-2
ISSN: 0076-6879

Publisher: Zoe Kruze
Editorial Project Manager: Saloni Vohra
Production Project Manager: James Selvam
Cover Designer: Gopalakrishnan Venkatraman
Typeset by MPS Limited, India

Contents

Section 2 Leveraging mononuclear non-heme iron enzymes for biocatalysis

Contributors

Gage T. Barroso
Department of Chemistry, University of Michigan, Ann Arbor, MI, United States

Jessica Lusty Beech
Department of Chemistry and Biochemistry, Montana State University, Bozeman, MT, United States

Zachary D. Bennett
Department of Chemistry, University of Wisconsin-Madison, Madison, WI, United States

Nora M. Bernet
Eawag, Swiss Federal Institute of Aquatic Science and Technology, Dübendorf; Institute of Biogeochemistry and Pollutant Dynamics (IBP), ETH Zurich, Zurich, Switzerland

Ambika Bhagi-Damodaran
Department of Chemistry, University of Minnesota – Twin Cities, Minneapolis, MN, United States

David G. Boggs
Department of Chemistry, University of Michigan, Ann Arbor, MI, United States

Charlotte E. Bopp
Eawag, Swiss Federal Institute of Aquatic Science and Technology, Dübendorf; Institute of Biogeochemistry and Pollutant Dynamics (IBP), ETH Zurich, Zurich, Switzerland

Jennifer Bridwell-Rabb
Department of Chemistry, University of Michigan, Ann Arbor, MI, United States

Thomas C. Brunold
Department of Chemistry, University of Wisconsin-Madison, Madison, WI, United States

Yuk Hei Cheung
Department of Chemistry, Boston University, Boston, MA, United States

Anoop Rama Damodaran
Department of Chemistry, University of Minnesota – Twin Cities, Minneapolis, MN, United States

Jennifer L. DuBois
Department of Chemistry and Biochemistry, Montana State University, Bozeman, MT, United States

Ran Duan
Department of Chemistry, University of Texas at San Antonio, San Antonio, TX, United States

Lindsay D. Eltis
Microbiology and Immunology, The University of British Columbia, Vancouver, BC, Canada

Julia Ann Fecko
The Huck Institutes of the Life Sciences, The Pennsylvania State University, University Park, PA, United States

Alejandro Arcadio Garcia
Department of Chemistry, University of Michigan, Ann Arbor, MI, United States

Robert R. Gipson
Department of Chemistry, Stanford University, Stanford, CA, United States

Clara Graves
Department of Chemistry, University of Pittsburgh, Pittsburgh, PA, United States

Mark W. Grinstaff
Department of Chemistry, Boston University, Boston, MA, United States

Thomas B. Hofstetter
Eawag, Swiss Federal Institute of Aquatic Science and Technology, Dübendorf; Institute of Biogeochemistry and Pollutant Dynamics (IBP), ETH Zurich, Zurich, Switzerland

Xiongyi Huang
Department of Chemistry, Johns Hopkins University, Baltimore, MD, United States

Kabirul Islam
Department of Chemistry, University of Pittsburgh, Pittsburgh, PA, United States

Madison Knapp
Department of Chemistry, University of Michigan, Ann Arbor, MI, United States

Jiasong Li
Department of Chemistry, University of Texas at San Antonio, San Antonio, TX, United States

Kelin Li
Department of Chemistry, Boston University, Boston, MA, United States

Aimin Liu
Department of Chemistry, University of Texas at San Antonio, San Antonio, TX, United States

Pinghua Liu
Department of Chemistry, Boston University, Boston, MA, United States

Hui Miao
Department of Chemical and Pharmaceutical Biology, Groningen Research Institute of Pharmacy, University of Groningen, Groningen, The Netherlands

Meredith B. Mock
Department of Chemical and Biological Engineering, The University of Alabama, Tuscaloosa, AL, United States

Sarah G. Pati
Department of Environmental Geosciences, Centre for Microbiology and Environmental Systems Science, University of Vienna, Vienna, Austria

Jinyan Rui
Department of Chemistry, Johns Hopkins University, Baltimore, MD, United States

Sandy Schmidt
Department of Chemical and Pharmaceutical Biology, Groningen Research Institute of Pharmacy, University of Groningen, Groningen, The Netherlands

Elizabeth R. Smithwick
Department of Chemistry, University of Minnesota – Twin Cities, Minneapolis, MN, United States

Edward I. Solomon
Department of Chemistry, Stanford University, Stanford; Stanford Synchrotron Radiation Lightsource, SLAC National Acceleration Laboratory, Stanford University, Menlo Park, CA, United States

Ryan M. Summers
Department of Chemical and Biological Engineering, The University of Alabama, Tuscaloosa, AL, United States

Megan E. Wolf
Microbiology and Immunology, The University of British Columbia, Vancouver, BC, Canada

Neela Yennawar
The Huck Institutes of the Life Sciences, The Pennsylvania State University, University Park, PA, United States

Shuyuan Zhang
Department of Chemical and Biological Engineering, The University of Alabama, Tuscaloosa, AL, United States

Tao Zhang
Department of Chemistry, Boston University, Boston, MA, United States

Qun Zhao
School of Biotechnology and Key Laboratory of Industrial Biotechnology of Ministry of Education, Jiangnan University, Wuxi, P.R. China

Niels A.W. de Kok
Department of Chemical and Pharmaceutical Biology, Groningen Research Institute of Pharmacy, University of Groningen, Groningen, The Netherlands

CHAPTER SEVEN

Unveiling the mechanism of cysteamine dioxygenase: A combined HPLC-MS assay and metal-substitution approach

Ran Duan, Jiasong Li, and Aimin Liu*
Department of Chemistry, University of Texas at San Antonio, San Antonio, TX, United States
*Corresponding author. e-mail address: Feradical@utsa.edu

Contents

Methods in Enzymology, Volume 703
ISSN 0076-6879, https://doi.org/10.1016/bs.mie.2024.05.018

Abstract

Mammalian cysteamine dioxygenase (ADO), a mononuclear non-heme Fe(II) enzyme with three histidine ligands, plays a key role in cysteamine catabolism and regulation of the *N*-degron signaling pathway. Despite its importance, the catalytic mechanism of ADO remains elusive. Here, we describe an HPLC-MS assay for characterizing thiol dioxygenase catalytic activities and a metal-substitution approach for mechanistic investigation using human ADO as a model. Two proposed mechanisms for ADO differ in oxygen activation: one involving a high-valent ferryl-oxo intermediate. We hypothesized that substituting iron with a metal that has a disfavored tendency to form high-valent states would discriminate between mechanisms. This chapter details the expression, purification, preparation, and characterization of cobalt-substituted ADO. The new HPLC-MS assay precisely measures enzymatic activity, revealing retained reactivity in the cobalt-substituted enzyme. The results obtained favor the concurrent dioxygen transfer mechanism in ADO. This combined approach provides a powerful tool for studying other non-heme iron thiol oxidizing enzymes.

1. Introduction

Thiol dioxygenases (TDOs) are a critical family of enzymes that play a vital role in regulating cellular thiol metabolism. These non-heme iron-dependent oxygenases, belonging to the Cupin superfamily, catalyze the oxidation of thiol-containing molecules into sulfinic acids (Aloi, Davies, Karplus, Wilbanks, & Jameson, 2019; Stipanuk, Simmons, Andrew Karplus, & Dominy, 2011). Cysteamine (2-aminoethanethiol, 2-AET) dioxygenase (ADO) and cysteine dioxygenase (CDO) are the only two enzymes that regulate thiol metabolism in mammalian cells by oxidizing thiol-bearing small molecules (Dominy, Simmons, Karplus, Gehring, & Stipanuk, 2006; Dominy et al., 2007). Cysteamine dioxygenase (ADO) stands out for its diverse substrate range. Unlike most TDOs, ADO oxidizes small organic thiols like cysteamine and targets *N*-terminal cysteine residues in signaling proteins or peptides involved in oxygen sensing (Gunawardana, Heathcote, & Flashman, 2022; Masson et al., 2019). This unique ability highlights the remarkable adaptability of ADO and underscores the need to further understand its reaction mechanism and dynamic structure.

Despite performing similar functions, ADO belongs to the PFam family PF07847 (PCO_ADO), which is distinct from PFam family PF05995 (CDO_I) that includes CDO and 3-mercaptopropionate dioxygenase (MDO). Like plant cysteine oxidases (PCO) in the PCO_ADO family, ADO also oxidizes *N*-terminal cysteine-containing signaling peptides that

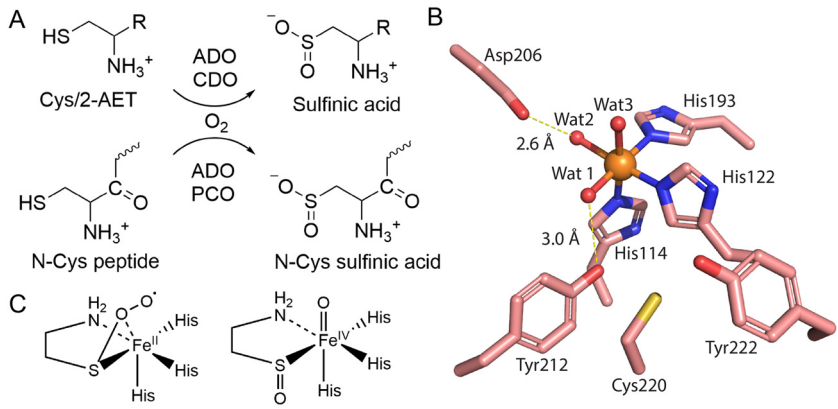

Fig. 1 The reaction, structure, and catalytic mechanism of ADO. (A) Thiol dioxygenase catalyzed reactions. *R* = H (ADO), $-COO^-$ (CDO); ADO and PCO catalyze certain *N*-terminal Cys-containing peptides and proteins. (B) Active site architecture of human ADO (Wang, Shin, Li, & Liu, 2021); (C) The key reaction intermediates in the two proposed mechanisms. Left: Concurrent dioxygen transfer intermediate. Right: High-valent ferryl-oxo intermediate.

are involved in oxygen-sensing (Gunawardana et al., 2022; Masson et al., 2019) (Fig. 1A). Therefore, ADO distinguishes itself by its broad spectrum of substrates, inserting oxygen atoms from the dioxygen molecule (O_2) into small organic thiol substrates, cysteamine, and large protein substrates. The dynamic structure of ADO, which accommodates two kinds of substrates with distinct sizes and structures, and the reaction mechanism are attractive topics in the emerging field of thiol dioxygenases.

Even though ADO has been purified from horse kidneys for more than 60 years (Cavallini, Scandurra, & De Marco, 1963; Cavallini, de Marco, Scandurra, Dupré, & Graziani, 1966), it was not genetically identified and heterologously expressed until 2007 (Dominy et al., 2007). Due to a relatively slow autooxidation, the mononuclear iron center in as-isolated ADO proteins has been shown to be present in mixed ferrous and ferric forms by EPR spectroscopy (Fernandez, Dillon, Stipanuk, Fox, & Brunold, 2020; Rotilio, Federici, Calabrese, Costa, & Cavallini, 1970; Wang et al., 2020). A Mössbauer spectroscopy study observed that 23% of iron is in the Fe(III) form in as-isolated mouse ADO (Wang et al., 2020). The heterogeneous metal oxidation state inevitably introduces an inhomogeneous coordination environment and corresponding variations in protein structure that are likely responsible for obstructing the crystallographic characterization of this protein for a long period of time. Even though the Fe

(II)-bearing mouse ADO has been crystallized (Fernandez et al., 2021), it has been challenging to obtain a high-quality crystal structure for Fe(II)-bearing human ADO. One method to overcome this technical challenge associated with the metal oxidation state is to swap the Fe center with a Ni ion, as we have done in a previous structural study (Wang, Li, & Liu, 2021). Along with the mutations of surface cysteine residues on ADO to suppress the expected nonhomogeneous disulfide bond formation, the crystal structure of human ADO has been successfully determined at 1.78 Å resolution (Wang, Li, & Liu, 2021) (Fig. 1B). This success inspired us to generate ADO proteins with different metal centers and take advantage of their unique chemical and physical properties to decipher the catalytic mechanism of ADO.

The catalytic mechanism of TDOs remains debatable despite substantial structural and spectroscopic research. Currently, two mechanisms have been proposed based on the extensive study of CDO, the founding member of this group of enzymes. The first proceeds via a non-ferryl-oxo-dependent concurrent dioxygen transfer to the thiol group of the substrate, while the second undergoes a more traditional oxygen activation mechanism involving a high-valent ferryl-oxo species and stepwise O atom transfers (Fig. 1C). The first mechanism was proposed based on a persulfenate intermediate (Driggers et al., 2013; Simmons et al., 2008). The second mechanism was solely proposed based on computational studies (Kumar, Thiel, & de Visser, 2011), while the attempts to trap the ferryl intermediate were not successful (Tchesnokov et al., 2016). Since a high-valent ferryl-oxo species is critical in the second mechanism, substituting iron for other metals that barely present a high-valent state in the enzyme is attractive for discerning between these two mechanisms.

Swapping Fe(II) for other divalent metals has been an important strategy to investigate the catalytic mechanisms of dioxygenases. In an iron-dependent dioxygenase, homoprotocatechuate 2,3-dioxygenase (HPCD), the cobalt-substituted enzyme maintains ring cleaving activity (Fielding, Lipscomb, & Que, 2012), suggesting that the oxidation state of cobalt during the catalysis also remains the same, like the natural iron enzymes (Lipscomb, 2014; Traore & Liu, 2022). In another Cupin-type enzyme, acireductone dioxygenase (ARD), Fe-ARD and Ni-ARD both present catalytic activity with different ARD isomers (Dai, Pochapsky, & Abeles, 2001). These studies imply that non-ferryl-oxo-dependent dioxygenases can maintain reactivity after proper metal swapping from Fe(II) to Co(II) or Ni(II).

In this chapter, we describe a new HPLC-mass spectrometry (HPLC-MS)-based ADO assay protocol in addition to the commonly used oxygen electrode-based ADO assay and the methods to prepare and study cobalt(II)-substituted ADO, Co(II)-ADO. The experimental methods include protein expression, purification, crystallization, spectral characterization, cobalt reconstitution, and a new high-performance liquid chromatography-mass spectrometry (HPLC-MS) analysis of the reaction product. Cell culture for Co(II)-ADO was conducted in minimal media supplemented with $CoCl_2$ during expression. As-purified Co(II)-ADO was characterized by optical and electron paramagnetic resonance (EPR) spectroscopy to confirm the presence of cobalt. We developed a method to prepare a close to metal-free "apo-ADO" form of the protein that uses chelating reagent treatment to eliminate the interference of trace amounts of metals. The cobalt-reconstituted ADO was prepared by incubating "apo-ADO" with $CoCl_2$. A ferrozine assay determined iron content in cobalt-reconstituted ADO, and the reactivity was precisely evaluated by an HPLC-MS method using isocratic elution. This cobalt-substitution method helps us gain insights into the natural iron-dependent thiol dioxygenases (Li, Duan, & Liu, 2024). A Cobalt(IV)-oxo species has not been observed in biology. All synthetic Co(IV)-oxo complexes require the support of a macrocyclic ligand set (Wang et al., 2017). Thus, if a cobalt-substituted non-heme enzyme is catalytically active, it would favor the pathway not involving a high-valent metal-oxo. The same strategy can be applied to the structural and mechanistic study of many other non-heme iron-dependent enzymes.

2. Protein expression, purification, and crystallization

This section describes the expression and purification of human ADO (hADO) with an iron or cobalt metal center. The wild-type (WT) hADO and hADO C18S/C239S were cloned to pET-28a-TEV expression vector plasmid with a cleavable His_6-tag containing 30 additional amino acids at the *N*-terminus in our previous work (Wang, Li, & Liu, 2021). *Escherichia coli* BL21 (DE3) competent cells were transformed with the plasmid. Cell culture was conducted in M9 medium with the supplement of Fe(II) or Co(II) to minimize the contamination of other metal ions. Fe-ADO was purified using an immobilized metal affinity chromatography (IMAC) column charged with nickel, while Co-ADO was purified using a cobalt IMAC column to prevent contamination with nickel ions. The *N*-terminal His-tagged ADO was mixed

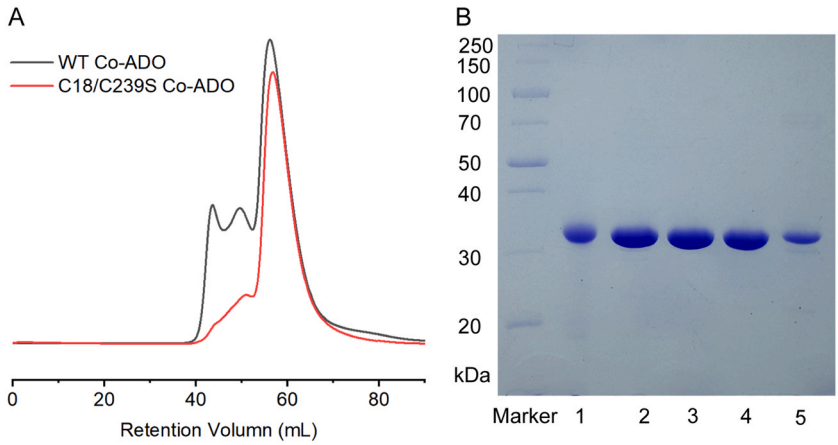

Fig. 2 Comparison of wild-type Co-ADO and C18S/C239S variant by gel filtration chromatography (A) and SDS-PAGE (B). (1) C18S/C239S Fe-ADO; (2) WT Fe-ADO; (3) C18S/C239S Co-ADO; (4) WT Co-ADO; and (5) "Apo-ADO".

with tobacco etch virus (TEV) protease and dialyzed against the dialysis buffer containing 10 mM tris(hydroxymethyl)aminomethane-HCl (Tris-HCl) (pH 8.0). The His_6-tag-cleaved and un-cleaved proteins were separated using the IMAC column. The non-tagged hADO proteins were further purified by gel filtration chromatography using Superdex 75. The purity of the proteins was evaluated using sodium dodecyl sulfate–polyacrylamide gel electrophoresis (SDS-PAGE). The hADO C18S/C239S mutant can be expressed, purified, and crystallized using the same method. ADO forms inter- and intra-disulfide bonds among subunits with two surface located cysteines, Cys18 and Cys239, causing heterogeneity (Wang et al., 2021). These two cysteine residues are not conserved in other thiol dioxygenases, and their mutation to serine does not affect the enzymatic activity of ADO. Compared to wild-type (WT) hADO, the C18S/C239S variant is more homogeneous and predominant in a monomeric form (Fig. 2A). After gel filtration chromatography, the purity of ADO proteins is suitable for future experiments (Fig. 2B).

2.1 Equipment

- Shaking incubator (Excella E25, New Brunswick Scientific).
- Cell disruptor (LM20 Microfluidizer Processor, Microfluidics International Corporation).
- Centrifuge (Avanti JXN-26, Beckman Coulter).

- Fast protein liquid chromatography (FPLC) (ÄKTA pure chromatography system, Cytiva).
- Ni-IMAC column (HisTrap HP, Cytiva).
- Gel filtration chromatography column (HiLoad 16/600 Superdex 75 prep grade, Cytiva).

2.2 Reagents

- Luria Broth (LB) Broth (Miller) medium: 10.0 g/L tryptone, 10.0 g/L NaCl, and 5.0 g/L yeast extract, sterilized by autoclave.
- M9 salt solution: 12.8 g/L Na_2HPO_4, 3.0 g/L KH_2PO_4, 0.5 g/L NaCl, and 1.0 g/L NH_4Cl, dissolved in double-distilled water (ddH_2O), sterilized by autoclave.
- 1 M $MgSO_4$ stock solution, sterilized by 0.22 μm filtration and stored at 4 °C.
- 1 M $CaCl_2$ stock solution, sterilized by 0.22 μm filtration and stored at 4 °C.
- M9 supplement buffer (50×): 200 g/L glucose, 20 g/L casamino acid, and 100 mg/L thiamine, sterilized by 0.22 μm filtration and stored at 4 °C
- Kanamycin stock solution: 50 mg/mL kanamycin dissolved in ddH_2O, sterilized by 0.22 μm filtration and stored at −20 °C.
- $CoCl_2$ stock solution: 0.1 M $CoCl_2$, dissolved in ddH_2O.
- $Fe(NH_4)_2(SO_4)_2$ stock solution: 0.1 M $Fe(NH_4)_2(SO_4)_2$ dissolved in ddH_2O, freshly prepared.
- Isopropyl β-d-1-thiogalactopyranoside (IPTG) stock solution: 1 M IPTG dissolved in ddH_2O, sterilized by 0.22 μm filtration and stored at −20 °C.
- Phenylmethylsulfonyl fluoride (PMSF).
- Lysing buffer: 50 mM Tris-HCl, 200 mM NaCl, pH 8.0, stored at 4 °C.
- Elution buffer: 50 mM Tris-HCl, 200 mM NaCl, 500 mM imidazole, pH 8.0, stored at 4 °C.
- Storage buffer: 50 mM Tris-HCl, 50 mM NaCl, pH 7.6, stored at 4 °C.
- Dialysis buffer: 10 mM Tris-HCl, pH 8.0, stored at 4 °C.
- TEV protease stock solution (2 mg/mL).
- Crystallization buffer: 100 mM Bis-Tris (pH 5.5), 200 mM $(NH_4)_2SO_4$, and 20% (w/v) PEG3350.

2.3 Procedure

1. Inoculate a single colony of competent cells to 5 mL LB medium with 50 mg/L kanamycin. Incubate this preculture at 37 °C, 220 rpm for 8 h.

2. Prepare M9 medium by mixing 200 mL of M9 salt solution, 4 mL of M9 supplement buffer, 0.2 mL of 1 M $MgSO_4$ solution, 0.02 mL of 1 M $CaCl_2$ solution, and 0.2 mL of kanamycin stock solution in a 1 L flask. Transfer 1 mL of preculture to the M9 medium and incubate at 37 °C, 220 rpm for 12 h.
3. Prepare M9 medium by mixing 1 L of M9 salt solution, 20 mL of M9 supplement buffer, 1 mL of 1 M $MgSO_4$ solution, 0.1 mL of 1 M $CaCl_2$ solution, and 1 mL of kanamycin stock solution in a 2 L baffled flask. Transfer 20 mL of preculture to the M9 medium and incubate at 37 °C, 220 rpm.
4. When the optical density at 600 nm (OD_{600}) reaches 0.4, add 0.2 mL of $Fe(NH_4)_2(SO_4)_2$ or $CoCl_2$ stock solution (20 μM final concentration) solution to the1 L culture.
5. When the OD_{600} reaches 0.8, add 0.5 mL of 1 M IPTG solution (0.5 mM final concentration) to induce gene expression. Incubate at 37 °C, 220 rpm for another 4 h.
6. Harvest cells by centrifugation for 10 min at 8000g, 4 °C. Freeze cell pellet at −80 °C for future use.
7. Resuspend the cell pellet in the lysing buffer with 2 mg PMSF supplement. Disrupt cells at 30,000 psi in the ice bath. Centrifuge for 1 h at 34,000g, 4 °C, to remove cell debris.
8. Assign lysing buffer as buffer A, and elution buffer as buffer B. Load the supernatant to the Ni or Co-IMAC column at 1 mL/min speed in the FPLC.
9. When loading is done, wash the column with two column volumes (CVs) of 100% buffer A. Then, wash the column with two CVs of 1% buffer B. Elute with 100% buffer B and collect ADO protein.
10. Concentrate down ADO protein and dilute in the lysing buffer to remove excess imidazole. Mix ADO protein and TEV protease in a 10:1 w/w ratio to cut the His_6 tag. Dialyze in 2 L dialysis buffer for 12 h at 4 °C.
11. Remove precipitate by centrifugation at 30,000g for 10 min. Load cut protein onto Ni or Co-IMAC columns at 1 mL/min speed. Collect the flow-through solution.
12. Concentrate down ADO protein to 2 mL aliquot. Equilibrate Superdex 75 column with the storage buffer. Purify ADO protein through Superdex 75 column using 1.5 mL/min speed at 4 °C. Collect purified ADO protein and freeze at −80 °C for future use.

13. Load 2 μg of protein in the well of a SDS-PAGE gel. Evaluate the purity of ADO protein by SDS-PAGE.
14. For protein crystallization, hADO C18S/C239S protein was concentrated to approximately 30 mg/mL and mixed at 1:1 (v/v) with a crystallization buffer using the hanging drop, vapor-diffusion method at 289 K.

2.4 Note

1. The cell membrane can be disrupted by sonication without influencing quality or yield.
2. The Co-IMAC column can be prepared by treating a regular Ni-IMAC column with the following solutions in sequence: 2 CV of ddH_2O, 4 CV of 0.1 M ethylenediaminetetraacetic acid (EDTA) solution, 2 CV of ddH_2O, 4 CV of 0.1 M $CoCl_2$ solution, and 2 CV of ddH_2O.
3. ADO purified through a Co-IMAC or Ni-IMAC column may contain cobalt and nickel ions because the iron binding is less tight than that of heme enzymes. However, this metal substitution has a negligible influence on preparing metal-substituted ADO proteins with the procedure of stripping metal ions prior to metal reconstitution.

3. Spectral characterization of Co-ADO

The Co-ADO from the M9 medium exhibits distinct spectroscopic properties. Co-ADO shows a light yellow color, whereas the "apo-ADO" is colorless. The Co(II) is EPR active with its d^7 electron configuration. In contrast, the Fe(II) in WT ADO is EPR silent with its d^6 electron configuration. In this section, we conducted a spectroscopic characterization of the Co(II)-ADO. The optical spectrum of Co(II)-ADO exhibits two strong shoulders at approximately 310 and 420 nm, and a much weaker shoulder in the 450–700 nm region. The spectrum is consistent with spectral features of Co(II)-ACMSD (Li, Walker, Iwaki, Hasegawa, & Liu, 2005), which is assigned as a pentacoordinate Co(II) center ligated via three His, one Asp, and one water. The optical spectral features are much more pronounced when shown as difference spectra over "apo-ADO" (Fig. 3A). The two stronger shoulders are due to the ligand-to-metal charge transfer (LMCT), which gives Co-ADO a light yellow color. The weaker shoulder in the 450−700 nm region is caused by the d-d transitions of the Co(II) ion. The relationship between the coordination number and the extinction

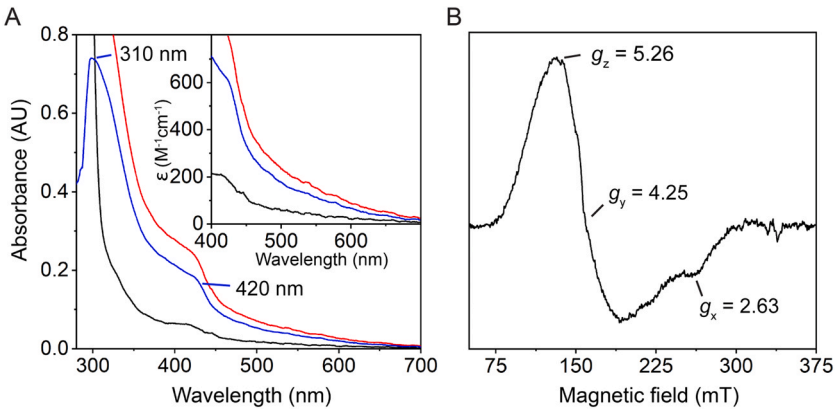

Fig. 3 The optical and EPR spectra of Co-ADO. (A) The optical spectra of 300 μM apo-ADO (black), Co-ADO (red), and their difference spectrum (blue). (B) The EPR spectrum of 100 μM Co-ADO. The EPR data was collected at 30 K with a microwave power of 3.17 mW.

coefficients of the d-d transitions in the visible region (450−750 nm) of high-spin Co(II) model complexes have been extensively discussed (Bertini & Luchinat, 1984; Horrocks, Ishley, Holmquist, & Thompson, 1980; Sellin, Eriksson, Aronsson, & Mannervik, 1983). General guidelines of this literature indicate that extinction coefficients for peaks between 400 and 900 nm are usually below 50 for six-coordination geometry, between 50 and 300 for five-coordination geometry, and greater than 300 for four-coordination geometry. The molar extinction coefficient at 550 nm is approximately 100 $M^{-1}cm^{-1}$, indicating a five-coordinated or highly distorted six-coordinate high-spin Co(II) center. These results revealed a distortion of the cobalt ligand environment away from an idealized six-coordinate geometry. As depicted in Fig. 3B, an as-isolated Co(II)-ADO exhibited a high-spin (HS) center, characteristic of a typical ground spin state of $S = 3/2$ Co(II) species with effective g values (g_x, g_y, g_z) of 2.63, 4.25, and 5.26. HS EPR spectra have been noted in Co(II)-ACMSD (Li et al., 2005) and Co(II)-QueD (Merkens, Kappl, Jakob, Schmid, & Fetzner, 2008), the effective g values of which differ from Co-ADO owing to the variation in ligated residues and coordination geometry.

3.1 Equipment

- X-band EPR spectrometer (E560 EPR/ENDOR spectrometer with a cryogen-free 4 K temperature system, Bruker Corporation).
- UV–vis spectrometer (Evolution Pro UV–vis Spectrophotometer, Thermo Fisher Scientific).

3.2 Reagents

- Storage buffer: 50 mM Tris-HCl, 50 mM NaCl, pH 7.6, stored at 4 °C.
- Co-ADO: As purified Co-ADO from M9 medium, dissolved in the storage buffer in aerobic conditions.
- Metal-strapped ADO: "apo-ADO" from Section 4.3, dissolved in the storage buffer in aerobic conditions after three rounds of buffer changing.

3.3 Optical spectral characterization

1. Turn on the UV–vis spectrometer and wait 30 min until the lamps are warmed up.
2. Set scan range from 250 to 800 nm. Scan the storage buffer as blank for all samples.
3. Scan the UV–vis spectrum of 300 μM Co-ADO or "apo ADO".
4. Determine the molar extinction coefficient.

3.4 EPR spectral characterization

1. Add 200 μL of 100 μM Co-ADO to an EPR quartz tube. Slowly freeze down the sample in liquid nitrogen. Store in a liquid nitrogen tank. Prepare a sample with storage buffer using the same method as the blank.
2. Set the EPR spectrometer at 100 kHz modulation frequency, 0.6 mT modulation amplitude, and wait for the temperature to decrease to 4.5 K.
3. Scan the blank sample's EPR spectrum using 3.17 mW microwave power at 30 K. Each spectrum averages four scans.
4. Scan the EPR spectrum of Co-ADO using 3.17 mW microwave power at 30 K. Each spectrum averages four scans.

4. Cobalt reconstitution in ADO

Even though Co-ADO is cultured in the M9 medium with minor metal ions, trace amounts of iron can still be detected in the Co-ADO from the EPR spectrum. To evaluate the role of cobalt in the ADO reactivity and spectroscopic properties, the proper method is to prepare near metal-free "apo-ADO" and compare the results before and after cobalt incorporation. However, removing metal ions from a non-heme iron-dependent protein is challenging. The three ligated histidine residues make the metal ion resistant to removal by regular EDTA treatment. Here we describe a method to carry out cobalt reconstitution on WT ADO using

1,10-phenanthroline as a chelating reagent (Ren, Lee, Wang, & Liu, 2022). The iron content in "apo-ADO" and Co-ADO was characterized using the ferrozine assay (Tchesnokov, Wilbanks, & Jameson, 2012). The reconstitution process was carried out in 4-(2-hydroxyethyl)-1-piperazineethanesulfonic acid (HEPES) buffer to reduce the interaction between buffer (i.e., Tris-HCl buffer) and metal ions.

4.1 Equipment

- Centrifuge (Avanti JXN-26, Beckman Coulter).
- FPLC (ÄKTA pure™ chromatography system, Cytiva).
- Desalting column (HiTrap Desalting, Cytiva).
- Hotplate and stirrer (IKA® C-MAG HS hotplate stirrers, IKA Inc.).
- UV–vis spectrometer (Evolution™ Pro UV–vis spectrophotometers, Thermo Scientific).
- Schlenk line.
- Vacuum pump.

4.2 Reagents

- HEPES buffer: 50 mM HEPES buffer, pH 8, stored at 4 °C.
- 1,10-phenanthroline stock solution: 0.1 M 1,10-phenanthroline in 0.1 M HCl.
- EDTA stock solution: 0.1 M EDTA solution, pH 8.
- $Na_2S_2O_4$ stock solution: 1 M $Na_2S_2O_4$, dissolved in ddH_2O, freshly prepared.
- $CoCl_2$ stock solution: 0.1 M $CoCl_2$, dissolved in ddH_2O.
- Ferrozine assay mixture: 5.56 mM ferrozine, 2.9% ascorbic acid, 430 mM ammonium acetate, pH 9.
- 80% H_2SO_4.
- Iron standard: 10 μL $Fe(NH_4)_2(SO_4)_2$ in HEPES buffer; 5 μL 80% H_2SO_4.

4.3 Preparation of "apo-ADO" through 1,10-phenanthroline assay

1. Degas 1.8 mL of 300 μM WT ADO protein with a Schlenk line for 30 min in the ice bath.
2. Add 4 μL of 1 M $Na_2S_2O_4$, 100 μL of EDTA stock solution, and 100 μL of 1,10-phenanthroline stock solution to the ADO protein. The final concentrations of reagents are 2 mM $Na_2S_2O_4$, 5 mM EDTA, and 5 mM 1,10-phenanthroline. Leave the ADO protein solution at 4 °C for 1 h until it reacts thoroughly. The solution should turn to an orange-red color.

3. Fill the desalting column with HEPES buffer. Load ADO protein to the desalting column at 5 mL/min speed and collect the first peak. Concentrate down protein solution into a 1.8 mL aliquot.
4. Repeat Steps 2 and 3 two more times.

4.4 Evaluation of the "apo-ADO" using ferrozine assay

1. Prepare the "apo-ADO" stock solution by concentrating the "apo-ADO" protein from Section 4.3 to millimolar concentration. Calculate the final concentration of the "apo-ADO" sample (1/15 of the apo-ADO stock solution).
2. Mix 10 μL of "apo-ADO" stock solution with 5 μL 80% H_2SO_4 in a centrifuge tube. Heat to 95 °C for 30 min using the hot plate.
3. After cooling down, add 135 μL of ferrozine assay mixture to the sample and mix well. Remove precipitate by centrifugation at 20,000g for 5 min
4. Add 10 μL of HEPES buffer and 5 μL of 80% H_2SO_4 to 135 μL of ferrozine assay mixture to make a blank sample. Measure the UV–vis absorbance at 562 and 750 nm. Use the absorbance at 750 nm as the baseline for all samples.
5. Add 15 μL of iron standard with different $Fe(NH_4)_2(SO_4)_2$ concentrations to 135 μL of ferrozine assay mixture. Measure the UV–vis absorbance at 562 nm (A_{562}). Repeat three times for each concentration of standard. Generate a standard curve of A_{562} vs. iron concentration.
6. Measure the UV–vis absorbance of the "apo-ADO" mixture at 562 nm. Fit the absorbance to the standard curve and determine the iron concentration in the "apo-ADO" mixture. Calculate the iron concentration and percentage in protein following the example in Fig. 4.

4.5 Reconstitution of ADO enzyme by adding divalent metal ions

1. Dilute "apo-ADO" to 50 μM in the desalting buffer.
2. Metal reconstitution method (using cobalt ion as an example): Add 0.1 M $CoCl_2$ stock solution to "apo-ADO" in drops while stirring at 4 °C, until the concentration of $CoCl_2$ reaches 50 μM.
3. Incubate the mixture at 4 °C for 30 min. Centrifuge at 20,000g for 2 min to remove precipitate. Use immediately for the HPLC-MS assay.

4.6 Note

- "Apo-ADO" protein is not stable. It is recommended to use it as soon as possible.
- The 1,10-phenanthroline stock solution should be made freshly within a month.

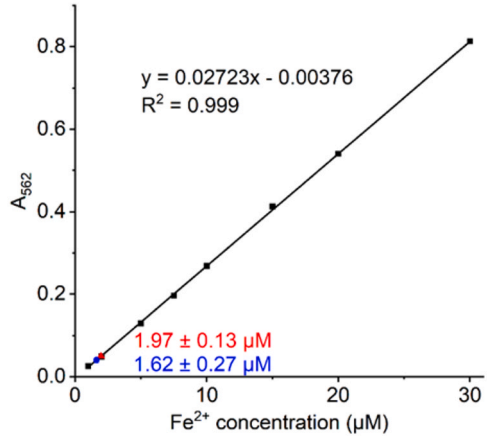

Fig. 4 Iron concentration determination of apo-ADO and Co-ADO produced from M9 media. The black trace shows the standard curve fitted by various concentrations of $Fe(NH_4)_2(SO_4)_2$. The iron concentration of 1.62 μM in 125 μM apo-ADO indicates that the iron occupancy is 1.30% (blue); The iron concentration of 1.97 μM in 114 μM Co-ADO indicates a 1.73% iron occupancy (red).

- To reduce the contamination of metal ions in the ferrozine assay, it is recommended that all glassware be acid-washed. The desalting buffer can be further purified using a Chelex 100 column.
- Each experiment should be performed in triplicate.
- The metal reconstitution method can be applied to other metal ions like Ni(II) or Fe(II). The Fe(II) reconstitution should be carried out in anerobic conditions.

5. HPLC-MS analysis of the hypotaurine formation by ADO

To determine the reactivity of "apo-ADO" and study the influence of cobalt on ADO, a precise method is required to identify the reaction product, hypotaurine, from its analogs in the activity assay. Even though the oxygen consumption of ADO reaction can be recorded using an oxygen electrode (Wang et al., 2018), the self-oxidization of cysteamine into the dimer form, cystamine, cannot be excluded from this method. A previously reported HPLC method can separate and detect hypotaurine efficiently (Coloso, Hirschberger, Dominy, Lee, & Stipanuk, 2006; Dominy et al., 2007). However, this coupled assay requires pre-treatment

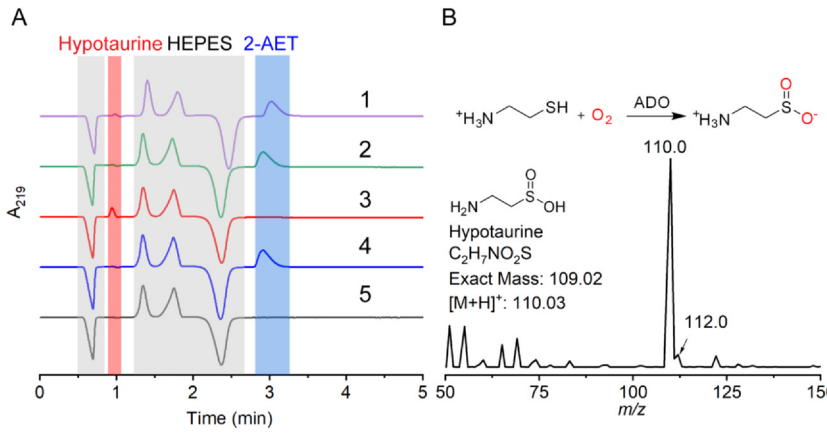

Fig. 5 (A) Demonstration of Ni(II)-ADO's dioxygenase catalytic activity and HPLC profile for ADO activity assay. (1) 50 μM reconstituted Ni(II)-ADO + 10 mM cysteamine; (2) 50 μM "apo-ADO" + 10 mM cysteamine; (3) HPLC hypotaurine sample; (4) HPLC cysteamine sample; and (5) HPLC blank sample. The details of the reaction setup are described in the text. The negative peak in the HPLC elution profiles emerged due to the difference between the reaction HEPES buffer in the samples and the HPLC solvent. (B) Reaction equation of ADO with cysteamine as a substrate and MS spectrum of the hypotaurine peak in Sample (3 of panel A).

with *o*-phthaldialdehyde and relies on an expensive fluorescence detector for detection. Inspired by the HPLC method used in the CDO activity assays (Li et al., 2018; McCoy et al., 2006), we developed a method using isocratic elution to separate hypotaurine from cysteamine directly. The hypotaurine product was verified using the retention time (Fig. 5A) and mass spectrum (Fig. 5B) of a commercially purchased standard. The reactivity of "apo-ADO" and Co-ADO can be determined through peak area integration.

5.1 Equipment

- HPLC system (UltiMate 3000 with diode array detector, Thermo Fisher Scientific).
- Analytical C18 column (Inertsil ODS-3 HPLC Column, 3 μm, 100 × 4.6 mm, GL Sciences Inc.).
- Ultra-centrifugal filter (Amicon Ultra Centrifugal Filter, 10 kDa MWCO, 0.5 mL, MilliporeSigma).
- Thermomixer (Thermomixer R, Eppendorf).

5.2 Reagents

- HPLC running buffer: 0.6% methanol, 0.3% Heptafluorobutyric acid (HFBA), and 99.1% dd H_2O.
- 6 M hydrochloride acid (HCl)
- HEPES buffer: 50 mM HEPES buffer, pH 8.
- Cysteamine stock solution: 1 M cysteamine (Purchased from Acros Organics), freshly prepared with degassed water (ddH_2O bubbled with N_2 gas).
- Hypotaurine stock solution: 50 mM hypotaurine dissolved in ddH_2O, freshly prepared.
- Hypotaurine standards: 200 μL of hypotaurine solutions at various concentrations, freshly prepared with ddH_2O and hypotaurine stock solution, filtered with 0.22 μm filter.
- HPLC blank sample: 198 μL of HEPES buffer; 2 μL 6 M HCl.
- HPLC cysteamine sample (10 mM): 196 μL HEPES buffer; 2 μL 6 M HCl; and 2 μL of 2-AET (1 M).
- HPLC hypotaurine sample (0.25 mM): 197 μL HEPES buffer; 2 μL 6 M HCl; and 1 μL 50 mM hypotaurine.
- "Apo-ADO" stock solution: 100 μM "apo-ADO", dissolved in HEPES buffer.
- Co-ADO stock solution: 100 μM Co-ADO generated from cobalt reconstitution (Section 4.5), dissolved in HEPES buffer.

5.3 Procedure

1. Wash the C18 column using the HPLC running buffer until the baseline turns flat.
2. Set up HPLC assay condition. Buffer: HPLC running buffer; Flow rate: 1.5 mL/min; Run time: 10 min; Wavelength: 219 nm; Injection volume: 50 μL.
3. Inject 50 μL of a hypotaurine standard and run HPLC assay. Repeat three times for each concentration of standard. Fit the peak area to the concentration as a standard curve.
4. Mix 100 μL of "apo-ADO" stock solution, and 96 μL of HEPES buffer in a microcentrifuge tube (tube A). Preheat to 37 °C on the thermomixer.
5. Add 2 μL of 1 M cysteamine to a 1.5 mL microcentrifuge tube (tube B), preheat to 37 °C on the thermomixer.
6. Add 2 μL of 6 M HCl to a 1.5 mL EP tube (tube C).
7. Transfer 196 μL of "apo-ADO" from tubes A to B to start the reaction. Set the thermomixer at 37 °C, 500 rpm. React for 2 min.

8. Transfer 198 μL of mixture from tubes B to C to quench the reaction.
9. Filter the reaction mixture with ultra-centrifugal filters at 10,000g for 10 min. Collect the flow-through as the "apo-ADO" sample. Final concentration: 50 μM "apo-ADO", 10 mM cysteamine.
10. Repeat steps 3–8 using Co-ADO stock solution. Collect the flow-through as the Co-ADO sample. Final concentration: 50 μM reconstituted Co-ADO, 10 mM cysteamine.
11. Inject 50 μL of HPLC blank sample and run HPLC assay.
12. Inject 50 μL of HPLC hypotaurine sample and run the HPLC assay. Determine the retention time of hypotaurine.
13. Inject 50 μL of HPLC cysteamine sample and run the HPLC assay. Calculate the peak area for hypotaurine. Set this peak area as the baseline for all samples.
14. Inject 50 μL of "apo-ADO" sample and run HPLC assay. Calculate the peak area for hypotaurine.
15. Inject 50 μL of Co-ADO sample and run HPLC assay. Calculate the peak area for hypotaurine.
16. Calculate the k_{obs} from the standard curve. Using the peak area values calculated from Steps 14 to 15, subtract the baseline from Step 13. Then fit the resultant values to the standard curve from Step 3 and convert them to the hypotaurine concentrations. The k_{obs} can be calculated from the formula below, where enzyme concentration is 50 μM and the reaction time is 2 min.

$$k_{obs} = \frac{\text{Hypoaturine concentartion}}{\text{Enzyme concentration} \times \text{Reaction time}}$$

5.4 Note

1. Make sure there are no leaks in the ultra-centrifugal filters. The unfiltered protein may clog the C18 column.
2. Cysteamine is hygroscopic and very easy to oxidize. It is recommended that cysteamine stock solution be stored in an O_2-free anaerobic chamber.
3. The 6 M hydrochloride acid is corrosive. Personal protective equipment (PPE) is required when handling it.
4. Each experiment should be performed in triplicate.
5. Regarding the iron-reconstituted ADO, the concentration of the ADO enzyme and Fe(II) needs to be reduced to 5 μM. Otherwise, most of the dissolved oxygen in the reaction mixture will be consumed, and the reactivity will be underestimated.

6. Summary and conclusions

This chapter presents a novel approach for investigating the catalytic mechanism of cysteamine dioxygenase (ADO) using metal substitution. We successfully generated cobalt(II)- and Ni-(II)-substituted ADO (Co-ADO and Ni-ADO) and characterized their properties. Optical and EPR spectroscopy confirmed cobalt incorporation into the enzyme, and the ferrozine assay verified the removal of the metal in apo-ADO after treatment. Importantly, the HPLC-MS method for activity assay demonstrates Co-ADO and Ni-ADO are catalytically competent and the dioxygenase activity of which is proportional to the amount of Co(II) or Ni(II) present. These combined results strongly support a non-ferryl-oxo-dependent, concurrent dioxygen transfer mechanism during ADO-mediated oxygenation. This work sheds light on thiolate-bound metalloenzyme oxygenation reactions and establishes a powerful method for studying other three-histidine non-heme iron enzymes oxidizing thiol-bearing substrates.

Acknowledgments

This work was supported by NSF award CHE-2204225. The use of HPLC was also partially supported by an administrative supplement of the NIH grant R01GM108988. A.L. acknowledges the support of Lutcher Brown's endowment and the Welch Foundation grant Welch AX-2110-20220331.

References

Aloi, S., Davies, C. G., Karplus, P. A., Wilbanks, S. M., & Jameson, G. N. L. (2019). Substrate specificity in thiol dioxygenases. *Biochemistry, 58*(19), 2398–2407.

Bertini, I., & Luchinat, C. (1984). High spin cobalt(II) as a probe for the investigation of metalloproteins. *Advances in Inorganic Biochemistry, 6*, 71–111.

Cavallini, D., de Marco, C., Scandurra, R., Dupré, S., & Graziani, M. T. (1966). The enzymatic oxidation of cysteamine to hypotaurine: Purification and properties of the enzyme. *Journal of Biological Chemistry, 241*(13), 3189–3196.

Cavallini, D., Scandurra, R., & De Marco, C. (1963). The enzymatic oxidation of cysteamine to hypotaurine in the presence of sulfide. *Journal of Biological Chemistry, 238*(9), 2999–3005.

Coloso, R. M., Hirschberger, L. L., Dominy, J. E., Lee, J.-I., & Stipanuk, M. H. (2006). Cysteamine dioxygenase: Evidence for the physiological conversion of cysteamine to hypotaurine in rat and mouse tissues. *Taurine, 6* (Boston, MA).

Dai, Y., Pochapsky, T. C., & Abeles, R. H. (2001). Mechanistic studies of two dioxygenases in the methionine salvage pathway of *Klebsiella pneumoniae*. *Biochemistry, 40*(21), 6379–6387.

Dominy, J. E., Simmons, C. R., Hirschberger, L. L., Hwang, J., Coloso, R. M., & Stipanuk, M. H. (2007). Discovery and characterization of a second mammalian thiol dioxygenase, cysteamine dioxygenase. *Journal of Biological Chemistry, 282*(35), 25189–25198.

Dominy, J. E., Simmons, C. R., Karplus, P. A., Gehring, A. M., & Stipanuk, M. H. (2006). Identification and characterization of bacterial cysteine dioxygenases: A new route of cysteine degradation for Eubacteria. *Journal of Bacteriology, 188*(15), 5561–5569.

Driggers, C. M., Cooley, R. B., Sankaran, B., Hirschberger, L. L., Stipanuk, M. H., & Karplus, P. A. (2013). Cysteine dioxygenase structures from pH4 to 9: Consistent cys-persulfenate formation at intermediate pH and a cys-bound enzyme at higher pH. *Journal of Molecular Biology, 425*(17), 3121–3136.

Fernandez, R. L., Dillon, S. L., Stipanuk, M. H., Fox, B. G., & Brunold, T. C. (2020). Spectroscopic investigation of cysteamine dioxygenase. *Biochemistry, 59*(26), 2450–2458.

Fernandez, R. L., Elmendorf, L. D., Smith, R. W., Bingman, C. A., Fox, B. G., & Brunold, T. C. (2021). The crystal structure of cysteamine dioxygenase reveals the origin of the large substrate scope of this vital mammalian enzyme. *Biochemistry, 60*(48), 3728–3737.

Fielding, A. J., Lipscomb, J. D., & Que, L. (2012). Characterization of an O_2 adduct of an active cobalt-substituted extradiol-cleaving catechol dioxygenase. *Journal of the American Chemical Society, 134*(2), 796–799.

Gunawardana, D. M., Heathcote, K. C., & Flashman, E. (2022). Emerging roles for thiol dioxygenases as oxygen sensors. *The FEBS Journal, 289*(18), 5426–5439.

Horrocks, W. D., Ishley, J. N., Holmquist, B., & Thompson, J. S. (1980). Structural and electronic mimics of the active site of cobalt(II)-substituted zinc metalloenzymes. *Journal of Inorganic Biochemistry, 12*(2), 131–141.

Kumar, D., Thiel, W., & de Visser, S. P. (2011). Theoretical study on the mechanism of the oxygen activation process in cysteine dioxygenase enzymes. *Journal of the American Chemical Society, 133*(11), 3869–3882.

Li, J., Griffith, W. P., Davis, I., Shin, I., Wang, J., Li, F., ... Liu, A. (2018). Cleavage of a carbon-fluorine bond by an engineered cysteine dioxygenase. *Nature Chemical Biology, 14*(9), 853–860.

Li, J., Duan, R., & Liu, A. (2024). Cobalt(II)-substituted cysteamine dioxygenase oxygenation proceeds through a cobalt(III)-superoxo complex. *Journal of the American Chemical Society* in press. https://doi.org/10.1021/jacs.4c01871.

Li, T., Walker, A. L., Iwaki, H., Hasegawa, Y., & Liu, A. (2005). Kinetic and spectroscopic characterization of ACMSD from *Pseudomonas fluorescens* reveals a pentacoordinate mononuclear metallocofactor. *Journal of the American Chemical Society, 127*(35), 12282–12290.

Lipscomb, J. D. (2014). Life in a sea of oxygen. *Journal of Biological Chemistry, 289*(22), 15141–15153.

Masson, N., Keeley, T. P., Giuntoli, B., White, M. D., Puerta, M. L., Perata, P., ... Ratcliffe, P. J. (2019). Conserved *N*-terminal cysteine dioxygenases transduce responses to hypoxia in animals and plants. *Science (New York, N. Y.), 365*(6448)), 65–69.

McCoy, J. G., Bailey, L. J., Bitto, E., Bingman, C. A., Aceti, D. J., Fox, B. G., & Phillips, G. N. (2006). Structure and mechanism of mouse cysteine dioxygenase. *Proceedings of the National Academy of Sciences, 103*(9), 3084–3089.

Merkens, H., Kappl, R., Jakob, R. P., Schmid, F. X., & Fetzner, S. (2008). Quercetinase QueD of *Streptomyces* sp. FLA, a monocupin dioxygenase with a preference for nickel and cobalt. *Biochemistry, 47*(46), 12185–12196.

Ren, D., Lee, Y.-H., Wang, S.-A., & Liu, H.-W. (2022). Characterization of the oxazinomycin biosynthetic pathway revealing the key role of a nonheme iron-dependent mono-oxygenase. *Journal of the American Chemical Society, 144*(24), 10968–10977.

Rotilio, G., Federici, G., Calabrese, L., Costa, M., & Cavallini, D. (1970). An electron paramagnetic resonance study of the nonheme Iron of cysteamine oxygenase. *Journal of Biological Chemistry, 245*(22), 6235–6236.

Sellin, S., Eriksson, L. E., Aronsson, A. C., & Mannervik, B. (1983). Octahedral metal coordination in the active site of glyoxalase I as evidenced by the properties of Co(II)-glyoxalase I. *Journal of Biological Chemistry, 258*(4), 2091–2093.

Simmons, C. R., Krishnamoorthy, K., Granett, S. L., Schuller, D. J., Dominy, J. E., Jr., Begley, T. P., ... Karplus, P. A. (2008). A putative Fe^{2+}-bound persulfenate intermediate in cysteine dioxygenase. *Biochemistry, 47*(44), 11390–11392.

Stipanuk, M. H., Simmons, C. R., Andrew Karplus, P., & Dominy, J. E. (2011). Thiol dioxygenases: Unique families of cupin proteins. *Amino Acids, 41*(1), 91–102.

Tchesnokov, E. P., Faponle, A. S., Davies, C. G., Quesne, M. G., Turner, R., Fellner, M., ... Jameson, G. N. L. (2016). An iron–oxygen intermediate formed during the catalytic cycle of cysteine dioxygenase. *Chemical Communications, 52*(57), 8814–8817. https://doi.org/10.1039/C6CC03904A.

Tchesnokov, E. P., Wilbanks, S. M., & Jameson, G. N. L. (2012). A strongly bound high-spin iron(II) coordinates cysteine and homocysteine in cysteine dioxygenase. *Biochemistry, 51*(1), 257–264.

Traore, E. S., & Liu, A. (2022). Charge maintenance during catalysis in nonheme iron oxygenases. *ACS Catalysis, 12*(10), 6191–6208.

Wang, B., Lee, Y.-M., Tcho, W.-Y., Tussupbayev, S., Kim, S.-T., Kim, Y., ... Nam, W. (2017). Synthesis and reactivity of a mononuclear non-haem cobalt(IV)-oxo complex. *Nature Communications, 8*, 14839.

Wang, Y., Davis, I., Chan, Y., Naik, S. G., Griffith, W. P., & Liu, A. (2020). Characterization of the nonheme iron center of cysteamine dioxygenase and its interaction with substrates. *Journal of Biological Chemistry, 295*(33), 11789–11802.

Wang, Y., Griffith, W. P., Li, J., Koto, T., Wherritt, D. J., Fritz, E., & Liu, A. (2018). Cofactor biogenesis in cysteamine dioxygenase: C−F bond cleavage with genetically incorporated unnatural tyrosine. *Angewandte Chemie International Edition, 57*(27), 8149–8153.

Wang, Y., Shin, I., Li, J., & Liu, A. (2021). *PDB entry 7REI: The crystal structure of nickel-bound human ADO C18S C239S variant*. https://doi.org/10.2210/pdb7REI/pdb.

Wang, Y., Shin, I., Li, J., & Liu, A. (2021). Crystal structure of human cysteamine dioxygenase provides a structural rationale for its function as an oxygen sensor. *Journal of Biological Chemistry, 297*(4), 101176.

Serial Editors

Anna Marie Pyle, Yale University, USA

David W. Christianson, University of Pennsylvania, USA

ACADEMIC PRESS

An imprint of Elsevier

elsevier.com/books-and-journals

ISBN 978-0-443-31304-2